The Astrophysical Journal, 882:101 (8pp), 2019 September 10 https://doi.org/10.3847/1538-4357/ab3394

Relativistic Sweet–Parker Current Sheet and Its Macroscopic Evolution

S. D. Yang[1,2]
[1] State Key Lab of Nuclear Physics and Technology and School of Physics, Peking University, Beijing 100871, People's Republic of China; sdyang@pku.edu.cn
[2] While visiting at PPPL, Princeton, NJ 08543, USA
Received 2019 February 9; revised 2019 July 12; accepted 2019 July 17; published 2019 September 6

Abstract

The problem of the relativistic Sweet–Parker current sheet is investigated, incorporating the effects of resistivity and thermal inertia. The scaling laws of the steady-state current sheet are obtained, and generalizations are carried out to include pair processes. We study the macroscopic evolutions of the spontaneous current sheet, including thinning, stretching, and both at the same time, which are critical for understanding the processes in an evolving current sheet.

Unified Astronomy Thesaurus concepts: Plasma astrophysics (1261); Magnetic fields (994); Relativity (1393)

1. Introduction

Magnetic reconnection is a critical phenomenon in plasma physics, and has been intensively explored for six decades due to its significant role in space and astrophysical environments as well as fusion devices (Parker 1957; Sweet 1958). In space environments, reconnection is prominent in enabling fast energy conversion from electromagnetic energy to plasma kinetic energy, thus producing highly energized particles and power law emissions (Guo et al. 2014; Sironi & Spitkovsky 2014). In astrophysical environments, reconnection plays an important role in sawtooth oscillations and disrupts the equilibrium (Kadomtsev 1975; Wesson 1990). In highly magnetized plasmas, i.e., where Alfvén velocity reaches the order of the speed of light, reconnection takes on relativistic characteristics. This is important in astrophysics, where relativistic reconnection is considered an underlying mechanism for the dissipation of electromagnetic energy and high-energy emissions in many environments, such as gamma-ray bursts (GRBs; Thompson 1994; Hurley et al. 1999; McKinney & Uzdensky 2012), pulsar wind nebula (PWNe; Lyubarsky & Kirk 2001; Sironi et al. 2016), jets of active galactic nuclei (AGNs; Duncan & Thompson 1992; Giannios 2010), blazer emissions (Sironi et al. 2015; Petropoulou et al. 2016), and even magnetar magnetospheres (Thompson & Duncan 1995; Harding & Lai 2006; Kaspi & Beloborodov 2017) and black hole magnetospheres (Koide & Arai 2008; Dexter et al. 2014). The magnetization in extreme astrophysical environments, i.e., the ratio of magnetic energy by the plasma enthalpy $\sigma \equiv B^2/h$, can reach as high as 10^3–10^6 (Lyutikov & Uzdensky 2003). High-β plasmas with manifest thermal effects, reaching mildly relativistic magnetization of order unity, on the other hand, are obtained in laboratory laser, high-energy-density plasma experiments (Zhong et al. 2010; Joglekar et al. 2014).

The establishment of relativistic reconnection theory has involved multiple approaches. Relativistic Sweet–Parker, as well as Petcheck, regimes have been addressed analytically (Lyutikov & Uzdensky 2003; Lyubarsky 2005; Comisso & Asenjo 2014; Yang 2017) and numerically (Zenitani & Hoshino 2008; Takahashi et al. 2011; Liu et al. 2015), showing the effects of Lorentz factor and inertia. Tearing instabilities (Komissarov et al. 2007), which are plasmoid instabilities (Del Zanna et al. 2016) in resistive MHD, have been explored in view of current sheet stability and fast reconnection. When it comes to three-dimensional reconnection, Kelvin–Helmholtz instability is found to be important, inducing turbulence and therefore turbulent reconnection (Lazarian et al. 2015; Takamoto et al. 2015). On the other hand, in extremely magnetized plasmas, the magnetic field exceeds the critical value $B_{cr} \sim 10^{13}$ G and exotic effects such as radiation friction, inverse Compton cooling, and QED processes (Beloborodov 2017; Bulanov 2017) influence the reconnection process, which further complicates the problem.

Despite substantial advances, there are still many fundamental issues demanding comprehensive and rigorous investigation. The problem of relativistic current sheets is among them. Modifications of thermal-inertia effect (Comisso & Asenjo 2014), and electric energy (Yang 2017) to the early resistive Sweet–Parker scaling laws (Lyutikov & Uzdensky 2003) have been made; however, the former did not address the high magnetization scenario, and the latter is restricted to resistive MHD. Particularly, the macroscopic evolution of a current sheet to a Sweet–Parker state is critical, as it helps us to understand the evolution into an equilibrium current sheet, as well as serves as an evolving background from which instabilities and other microprocesses stem, a problem that remains unresolved in analytic theories of relativistic regimes.

To be comprehensive, here we focus on the relativistic Sweet–Parker current sheet. The scaling relation of the Sweet–Parker current sheet with different magnetizations is addressed in Section 2, taking into account the thermal-inertia effect. In Section 3, pair processes such as annihilation, radiation, and inverse Compton scattering are incorporated into the fluid model. Section 4 focuses on the macroscopic evolution of the current sheet in the absence of instabilities, with nonideal effects taken into account; and the evolution of the current sheet in general, with fixed length or constant width, are discussed separately. Section 5 provides our conclusions. In this paper we adopt the natural unit where the speed of light $c = 1$, and our discussions are in the context of special relativity.

2. Relativistic Sweet–Parker Current Sheet

Sweet–Parker reconnection, where magnetic fields with opposite directions are brought into contact by plasma flows and reconnect to release free energy encoded in the magnetic configuration, was the first proposed reconnection scenario due

to its conciseness. It was also studied when reconnection was extended to different plasma systems and relativistic regime, where new effect influences can be explicitly estimated. Here, therefore, we derive the Sweet–Parker-like scaling laws based on Koide's equations (Koide 2009). In a relativistic Sweet–Parker current sheet, the inflow is magnetically dominated, whereas the outflow is usually dominated by kinetic energy. The proportion of thermal energy and bulk kinetic energy of the outflow, however, depends on the detailed dynamics. Ohm's law contains irreversible dissipative terms as well as reversible collisionless terms. The former leads to a preferred conversion to bulk energy, and therefore a prominent increase in the thermal inertia of the outflow, whereas domination of the latter leads to particle acceleration, and manifests as relativistic fast outflow. Relativistic jets, usually conjectured as produced by reconnection, can have a Lorentz factor $\gamma \sim 2$–10 in n X-ray binary and $\gamma \sim 10$–20 in an AGN (Miller-Jones et al. 2006), sometimes even reaching 400 or higher in some GRBs (Vergani 2007). Assume thermalization to be described by relativistically defined enthalpy $h = mnH_s(\frac{p}{\rho})$, where m is the electron mass, n is the proper particle number density, p is the proper pressure, and ρ is the mass density. The Ohm's law in Koide's paper (Koide 2009) can then be reduced to

$$\eta J^{\mu} + \frac{1}{4q}\partial_{\nu}\left[\frac{h}{q}(U^{\mu}J^{\nu} + J^{\mu}U^{\nu})\right] = U_{\nu}F^{\mu\nu}. \tag{1}$$

Here U is the four-velocity of the fluid, η is the resistivity, $q = ne$ the latent charge density with n as the particle density of the plasma, and J is the four-velocity. Estimated in the rest frame of the current layer where thermal inertia contributes as $\partial_{\nu}[hJ^{\mu}U^{\nu}/q] \sim h\gamma_{\rm out}v_{\rm out}J^{\mu}/(Lq)$, the above equation gives

$$(\eta + d^2\gamma_{\rm out}v_{\rm out}/L)J^{\mu} = U_{\nu}F^{\mu\nu}, \tag{2}$$

where $v_{\rm out}$ and $\gamma_{\rm out}$ are the three-velocity and Lorentz factor of the outflow, respectively, L is the current sheet length, and the skin depth is $d = \sqrt{h/(4q^2)}$.

The proof is as follows: assume the proper densities of the plasma upstream and downstream to be of the same order, which is verified by Liu et al. (2015); in the absence of pair production, we have the balance relation $n_{\rm in}\gamma_{\rm in}v_{\rm in}L = n_{\rm out}\gamma_{\rm out}v_{\rm out}\delta$. Under the assumptions, this results in $v_{\rm in}L = \gamma_{\rm out}\delta$, and in the limit where plasma is thermalized, $h_{\rm out} \gg h_{\rm in}$, therefore $\frac{h_{\rm in}\gamma_{\rm in}v_{\rm in}}{\delta} \ll \frac{h_{\rm out}\gamma_{\rm out}v_{\rm out}}{L}$. The opposite limit where the enthalpy density outflow is not increased at all, $\frac{h_{\rm in}\gamma_{\rm in}v_{\rm in}}{\delta} = \frac{h_{\rm out}\gamma_{\rm out}v_{\rm out}}{L}$, and the thermal-inertia contribution to the nonideal electric field is still of the same order, modified by a factor 2. Assuming a steady-state uniform electric field $(\eta + \frac{d^2}{L}\gamma_{\rm out}v_{\rm out})J = E$, we can get the estimation $E = v_{\rm in}B_0$, where $\delta \sim B_0/J$.

The conservation properties between inflow and outflow shall be employed, of which the most important are the energy and momentum balance. For the energy flow

$$B_{\rm in}^2 v_{\rm in}L \approx h_{\rm out}\gamma_{\rm out}\delta. \tag{3}$$

And pressure balance across the current layer gives $p \sim B^2$; whereas the momentum equation is

$$\nabla_{\nu}\left[h\left(U^{\mu}U^{\nu} + \frac{1}{(2q)^2}J^{\mu}J^{\nu}\right)\right] = -\nabla^{\mu}p + J^{\nu}F^{\mu}{}_{\nu} \tag{4}$$

along the current sheet in the x direction

$$\partial_x(h\gamma_{\rm out}^2 v_{\rm out}^2) = -\partial_x p, \tag{5}$$

which leads to $h\gamma_{\rm out}^2 v_{\rm out}^2 \sim p$, where the magnetic field is negligible and pressure balance accelerates the outflow. Combining the two balance equations, we have

$$h\gamma_{\rm out}^2 v_{\rm out}^2 \sim B^2, \tag{6}$$

from which

$$\delta/L \sim v_{\rm in}/(\gamma_{\rm out}v_{\rm out}). \tag{7}$$

Combined with the expressions for the electric field and that for the current sheet width, the scaling relation can be expressed as

$$\frac{\delta}{L} \sim \left(\frac{\eta}{L\gamma_{\rm out}v_{\rm out}} + \frac{d^2}{L^2}\right)^{1/2}. \tag{8}$$

For an outflow of order unity, and expressing the four-Alfvén velocity as the square root of the inflow magnetic energy by the outflow enthalpy, the scaling relation becomes

$$\delta/L \sim (S^{-1} + d_L^2)^{1/2}, \tag{9}$$

where $S = L\sqrt{B_{\rm in}^2/h}/\eta$ and $d_L = d/L$. Here the inflow magnetic energy is assumed to be mainly converted into bulk kinetic energy, which is suggested by numerical simulations showing prominent nonthermal particles. Concerning the strength of nonideal terms, as discussed in Comisso & Asenjo (2014), the thermal-inertia effect becomes relevant when $d^2/L \geqslant \eta$, that is, the thermal-inertial layer width $\delta_{\rm ti} \sim d$ is of the same order or larger than the resistive layer width $\delta_{\eta} \sim S^{-1/2}L$, which depends on the thermal to electron rest mass energy ratio and the resistive nonidealness of the plasma.

3. Sweet–Parker Current Sheet with Pair Processes

Although current research mainly focuses on collisionless PIC simulations (Guo et al. 2014; Sironi & Spitkovsky 2014; Liu et al. 2015) for reconnections in pair plasmas, theoretical studies show that the mechanism for resistivity of pair plasmas is essentially different from that of electron-ion plasmas (Ruffini et al. 2010). In a wide range of parameters, electron-ion plasmas can be seen as collisionless, and the mechanism for resistivity is the Coulomb scattering described by a Rutherford cross section. On the contrary, for pair plasmas, collisions are always essential; even if the plasma itself can be considered classical, interactions are described by quantum cross sections. Unlike the classical case, the non-classical resistivity does not decrease with temperature. Due to the significance of quantum processes in pair plasmas, research is being conducted to address radiation and inverse Compton scattering in reconnection (Werner et al. 2019; Zhang et al. 2018).

In astrophysical plasmas, pair production and annihilation are ubiquitous processes (Lightman 1982; Arons 1983; Guilbert & Stepney 1985) when thermal energy is relativistic or plasma dynamics is drastic. Magnetic pair production (Erber 1966;

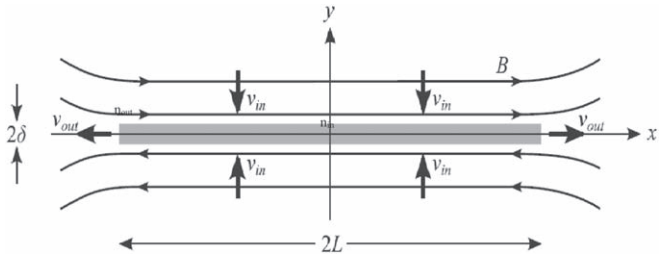

Figure 1. Sweet–Parker current sheet.

Daugherty & Harding 1983), $\gamma B \rightarrow e^+ + e^-$, is the dominant process of pair production for $B \geqslant 10^{12}$ G, where high-energy photons interact with a magnetic field to create pairs. In astrophysical environments, relativistic reconnection usually results in pair production, which may then lead to emissions (Beloborodov 2017) and give feedback on reconnection (Uzdensky 2011). In highly magnetized plasmas with $B \sim 10^{12}$ G or higher, beams with a Lorentz factor of order 10^6 are thought to undergo pair creation, leading to a multiplicity (the ratio of pair density to the ion density, normalized with respect to the initial value) of 10^2 and even 10^4 for $B \sim 10^{13}$ G or higher (Arendt & Eilek 2002). In relativistic reconnection, pair processes therefore will have significant effects on the large-scale balance relations, as well as affect the dynamics through Ohm's law. In this section, to have an idea of the role played by pair processes in reconnection, we study them in the Sweet–Parker model.

The conservation laws change due to variation in lepton number as well as energy losses upstream and downstream. Given an upstream condition, self-consistent calculation of the downstream parameters involves detailed dynamics, which is beyond the scope of the present discussion. However, we can still discuss the effects of the pair processes with phenomenological models, understanding how the additional effects influence reconnection. A simple model can be constructed as follows: (1) the inflow and outflow plasmas far from the diffusion region are assumed to be in thermal and pair equilibrium, with the properties of the plasmas described by macroscopic parameters. (2) The diffusion region, on the other hand, undergoes dynamic evolution, resulting in thermal inequilibirum, pair processes, and radiative processes. (3) The plasma parameters therefore change from the inflow to the outflow, manifested by a changed particle number density, enthalpy, and therefore thermal inertia and resistivity. See Figure 1.

Adopting the description from previous fluid theories of relativistic pair plasma (Gedalin 1996; Berezhiani et al. 2004), the conservation laws of particle flux as well as energy momentum flux can be modified, and the contributions of Coulomb collision, annihilation, anomalous resistivity, and Compton scattering are accounted for by the collisional operator and therefore appear in the effective resistivity. The particle flux conservation becomes

$$\partial_\mu N^\mu = -DN, \tag{10}$$

where $DN = DN^{(p)} + DN^{(a)}$ is the particle number density variation, where the first term results from pair production, and the second term is due to annihilation.

On the other hand, the momentum relation is

$$\partial_\nu T^{\mu\nu} = qN_\nu F^{\mu\nu} - DP^\mu, \tag{11}$$

where $DP^\mu = DP^{(c)\mu} + DP^{(a)\mu} + DP^{(p)\mu} + DP^{(an)\mu} + DP^{(\gamma)\mu} + DP^{(r)\mu}$ consists of the influence of Coulomb collision $DP^{(c)\mu}$, pair annihilation and production $DP^{(a)\mu}$, Compton scattering $DP^{(p)\mu}$ and anomalous resistivity $DP^{(an)\mu}$, whose detailed expressions are

$$\begin{aligned} DP_s^{(c)\mu} &- \sum_{s'\neq s} n_s n_{s'} \frac{m_s m_{s'}}{m_s + m_{s'}} \sigma_{ss'}^{(c)} F_{ss'} (u_s^\mu - u_{s'}^\mu) \\ DP^{(a)\mu} &= -\sum_{s'=-s} n_s n_{s'} \sigma_{ss'}^{(a)} F_{ss'} \\ DP_{s\gamma}^\mu &= -\sigma_{s\gamma} n_s n_\gamma m_s (u_s^\mu - u_\gamma^\mu) \\ DP^{(an)\mu} &= -\nu_s^{(an)} (u_s^\mu - U_0^\mu), \end{aligned} \tag{12}$$

where the subscripts indicate the sum over different species. n_s is the number density in the rest frame, $\sigma_{ss'}$ is the invariant cross section, and $F_{ss'} = \sqrt{(u_s \cdot u_{s'})^2 - 1}$ is the invariant flux. The anomalous resistivity is due to scattering on the turbulence and $\nu_s^{(an)}$ is the corresponding collision frequency. Compton scattering and pair photon-production are significant when there's a suitable photon background. When the radiative background is strong, annihilation can be balanced by photoproduction.

These different processes also have manifest influence on the nonideal electric field, as reflected by the resistive term in Ohm's law where

$$\eta_{\rm eff} = \eta^{(c)} + \eta^{(a)} + \eta^{(an)} + \eta_\gamma, \tag{13}$$

where $\eta^{(c)} = \frac{nm}{n_0 e^2}\sigma^{(c)}F$ is the Coulomb resistivity, $\eta^{(a)} = \frac{nm}{2n_0 e^2}\sigma^{(a)}F$ is from annihilation, $\eta^{(an)} = \frac{\nu^{(an)}}{nn_0 e^2}$ is due to anomalous resistivity, and $\eta_\gamma = \frac{n_\gamma m}{n_0 e^2}\sigma_\gamma$ comes from Compton scattering, respectively. The resistivity is determined by Coulomb collisions and annihilation cross sections in a dilute plasma without a photon background; and in the opposite situation, the resistivity is determined by the Compton scattering cross section and photon density. In contrast, in the pulsar magnetosphere, the pair plasma is almost collisionless (Manchester & Taylor 1977).

Phenomenologically, the overall contributions of the new terms can therefore be represented by an effective resistivity and a net particle source. From particle conservation, upon integration over the current sheet, with Gauss' law and the monotonicity of the third dimension,

$$n_{\rm in}\gamma_{\rm in}v_{\rm in}L - n_{\rm out}\gamma_{\rm out}v_{\rm out}\delta = \iint D_N dxdy. \tag{14}$$

Following the discussions, pair processes can be included in the model through lepton multiplicity M^l, effective resistivity $\eta_{\rm eff}$, and the density of energy loss $P_{\rm loss}$, where the parameters are given by

$$M_l = \frac{1}{1 + \iint D_N dxdy \big/ (n_{\rm out}\gamma_{\rm out}v_{\rm out}\delta)}, \tag{15}$$

$$P_{\rm loss} = \iint DP^0 dV. \tag{16}$$

The conservation relations can therefore be reorganized as

$$\gamma_{\rm in} v_{\rm in} n_{\rm in} L = \gamma_{\rm out} v_{\rm out} n_{\rm out} \delta / M^l. \quad (17)$$

In the absence of compression and expansion during the process, assuming nonrelativistic inflow and relativistic outflow, Equation (17) can be simplified as

$$v_{\rm in} L = \gamma_{\rm out} v_{\rm out} \delta / M^l. \quad (18)$$

And the energy balance becomes

$$B_{\rm in}^2 v_{\rm in} L \approx (\gamma_{\rm out} h_{\rm out} + P_{\rm loss})\delta. \quad (19)$$

Again, the inflow is assumed to be dominated by magnetic energy and the outflow is assumed to be dominated by kinetic energy. In this model, even if the outflow plasma is not thermalized at all, the possible multiplicity increase will enhance the thermal inertia significantly. In fact, pair production is an effective way of cooling, as is Compton scattering. Hence, reconnection increases the enthalpy of the outflow through two possible ways: (1) increasing thermal energy or (2) increasing the number of pairs. The two ways are related to different mechanisms for resistivity, where the latter is prone to having larger *Spitzer* resistivity. Also, the proportion of radiation in these two scenarios can be different, thus impacting the observable effect.

With the effective resistivity $\eta_{\rm eff}$ and the generalized Ohm's law, we can estimate the current

$$(\eta_{\rm eff} + d^2 \gamma_{\rm out} v_{\rm out}/L) J^\mu = U_\nu F^{\mu\nu}. \quad (20)$$

From the momentum balance, taking into account the momentum loss, which is integrated to be the energy loss, we can obtain

$$(h\gamma_{\rm out}^2 v_{\rm out} + P_{\rm loss})\gamma_{\rm out} \sim B^2. \quad (21)$$

Since the energy-loss term contributes both to the energy balance as well as the momentum balance, the same relation is obtained as in Section 2

$$\delta/L \sim v_{\rm in}/(\gamma_{\rm out} v_{\rm out}). \quad (22)$$

Similarly, we get the scaling relation

$$\frac{\delta}{L} \sim \left(\frac{\eta_{\rm eff}}{L\gamma_{\rm out} v_{\rm out}} + \frac{d^2}{L^2}\right)^{1/2}. \quad (23)$$

These discussions are for the assumed Sweet–Parker current sheet, if achievable. Our results here show how the pair processes may affect this process, while the detailed dynamics and the proportion and magnitude of contribution from the pair processes rely on concrete parameter regimes. In real scenarios, pair processes are likely to lead to drastic dynamics, and as a result, highly nonuniform density and resistivity profiles could form, possibly leading to gravitational and rippling modes (Priest & Forbes 2000), which further complicate the dynamics.

4. The Evolution of Relativistic Current Sheets

Generically, current sheets with smaller aspect ratios may form and evolve into Sweet–Parker sheets when the momentum balance is unable to sustain the initial aspect ratio and instabilities are too slow to destroy the current sheet during the evolution. This is an important process because many phenomena may happen during the current sheet evolution instead of after the Sweet–Parker equilibrium has already established. The macroscopic evolution of a current sheet is generic and has been observed in simulations where different setups may lead to different paths, i.e., thinning of width in Huang et al. (2017) and lengthening in Tenerani et al. (2016). In this section, we address the problem of spontaneous current sheet evolution in a relativistic regime, where different scenarios, i.e., free-evolving, fixed length, or fixed width, shall be explored.

Analytically, nonrelativistic spontaneous current sheet thinning was addressed in Kulsrud (2005) with constant length. The evolution of current sheet width there is investigated in an MHD framework, employing the balance of heat production, with ohmic heating and adiabatic heating, combined to give the total pressure change

$$-\int PdV + \int \boldsymbol{E}\cdot\boldsymbol{J}Vdt = PV, \quad (24)$$

which takes the form

$$\frac{L}{v_{\rm A}}\left(-p\frac{d\delta}{dt}\right) + p\left(\frac{\delta_{\rm SP}}{\delta}\right)^2 \delta = \Delta p \delta, \quad (25)$$

where $\delta_{\rm SP}$ is the width predicted by Sweet–Parker scaling given fixed L. The thinning is therefore

$$\delta^2 - \delta_{\rm SP}^2 = (\delta_0^2 - \delta_{\rm SP}^2) e^{-2t/\tau_{\rm A}}, \quad (26)$$

where $\tau_{\rm A} = L/v_{\rm A}$ is the Alfvén timescale characterizing the process of current sheet thinning. Note that this timescale is set by the macroscopic length of the system, due to the macroscopic nature of the evolution.

Relativistically, contributions from new terms and the effect of Lorentz transformation between the current sheet and moving fluid element are expected. With the thermal inertia effect included, ohmic heating is replaced by nonideal heating $\boldsymbol{E}\cdot\boldsymbol{J}$, i.e., $(\eta + \frac{d^2}{L}\gamma_{\rm out} v_{\rm out})\frac{B_0^2}{\delta^2}$, that is seen in the rest frame of the plasma. When the plasma element travels relativistically along the current sheet, the nonideal heating time should be $L/(\gamma_{\rm out} v_{\rm out})$. The plasma element or the nonideal heating rate should be Lorentz-transformed to ensure consistency, and either interpretation leads to the modification of gamma factor. On the other hand, gamma modification is not needed for the adiabatic heating time seen in the current sheet frame. The differences between the relativistic and nonrelativistic expression in nonideal heating and the Sweet–Parker scaling counteract and nonideal heating finally takes the form $\frac{\delta_{\rm SP}^2}{\delta^2}p$. Note that here $\delta_{\rm SP}$ is the width predicted for length L by the relativistic Sweet–Parker scaling law.

In the constant length scenario, the equations then can be reformulated as

$$\frac{d\delta}{dt} = \frac{v_{\rm out}}{L}\frac{\delta_{\rm SP}^2}{\delta} - \frac{v_{\rm out}}{L}\delta. \quad (27)$$

This looks the same as the nonrelativistic expression. Despite the differences between the detailed expressions, the similarity reveals the common nature of the relativistic and nonrelativistic current sheet evolution. As discussed above, the Lorentz effect is absorbed by the definition of relativistic Alfvén time, and thermal inertia enters into δ_{SP}, which represents the expected Sweet–Parker width for the initial length L. The first term on

the rhs is the diffusive expansion, while the second term is a decrease due to convection. For a given length, if a current sheet is much wider than the Sweet–Parker current sheet, the first term should be small, and the initial evolution is near ideal. As thinning goes on, the first term begins to be important and thinning slows down until the achievement of a Sweet–Parker aspect ratio. The solution is

$$\delta^2 - \delta_{\rm SP}^2 = (\delta_0^2 - \delta_{\rm SP}^2)e^{-2v_{\rm out}t/L} = (\delta_0^2 - \delta_{\rm SP}^2)e^{-2t/\tau}. \quad (28)$$

When the outflow velocity is of order unity, the characteristic time τ in current sheet rest frame is therefore L in natural units. In the collisionless limit, the final aspect ratio is set by the electron skin depth.

However, this discussion is under the assumption of fixed current sheet length, which is not necessarily the case. In the absence of constraints, i.e., fixed end points, the adjustment of the aspect ratio due to an inability to sustain a steady state can be achieved both by current sheet width thinning and length stretching, therefore a complete equation describing this kind of current sheet evolution should be

$$\frac{L}{v_{\rm out}}\left(-\frac{p}{\delta}\frac{d\delta}{dt}\right) + p\left(\frac{\eta L}{\gamma_{\rm out}v_{\rm out}} + d^2\right)/\delta^2 = p - \frac{L}{v_{\rm out}}\left(\frac{p}{L}\frac{dL}{dt}\right). \quad (29)$$

Given an initial condition, this equation describes the self-consistent evolution of the current sheet width and length. Transform it into

$$\frac{1}{\delta}\frac{d\delta}{dt} - \frac{1}{L}\frac{dL}{dt} = \frac{\eta}{\gamma_{\rm out}\delta^2} + \frac{d^2}{\delta^2}\frac{v_{\rm A}}{L} - \frac{v_{\rm A}}{L}. \quad (30)$$

The rhs is the difference between the timescale of thinning and lengthening, i.e., $d(\ln(\delta/L))/dt$. Evidently, initially for a current sheet with an aspect ratio much larger than Sweet–Parker, the first and second terms are negligible and, this difference is therefore the negative inverse Alfvén time. When the current sheet is near Sweet–Parker, the difference becomes tiny and the evolution is slow.

Assuming fixed width instead, as is the case for channel flows driven by magnetorotational instability (MRI) in accretion disks (Goodman & Xu 1994; Pessah 2010), we obtain the equation for the evolution of current sheet length:

$$\frac{dL}{dt} + \frac{\eta L}{\gamma_{\rm out}v_{\rm out}\delta^2} - v_{\rm out}(1 - d^2/\delta^2) = 0, \quad (31)$$

with the solution

$$L = [L_0 - \gamma_{\rm out}v_{\rm out}\delta^2(1 - d^2/\delta^2)/\eta]e^{-\eta t/\delta^2\gamma_{\rm out}} + \gamma_{\rm out}v_{\rm out}\delta^2(1 - d^2/\delta^2)/\eta. \quad (32)$$

Roughly, the timescale for thinning is the Alfvén timescale (light traveling time), while that for lengthening is the microscopic resistive time enhanced with the outflow Lorentz factor, due to the time dilation of the comoving plasma. If the microscale resistive time is to be equal to the macro-scale Alfvén travel time, then $\delta^2/\eta \sim L/v_{\rm A}$, which leads to the scaling of the aspect ratio:

$$\frac{\delta}{L} \sim S^{-1} = S_L^{-1/2}. \quad (33)$$

This is exactly the resistive Sweet–Parker scaling. And the same result can be obtained by simply equaling Equation (30) to 0.

Taking the collisional and the collisionless limits, we get $L = [L_0 - \gamma_{\rm out}v_{\rm out}\delta^2/\eta]e^{-\eta t/\delta^2\gamma_{\rm out}} + \gamma_{\rm out}v_{\rm out}\delta^2/\eta$ and $L = v_{\rm out}(1 - d^2/\delta^2)t$, respectively. Notably, in the collisionless limit the evolution of current sheet length cannot be independent of thinning without the entrance of other processes, as inertia here tends to expand the length linearly. This is a clear demarcation between the collisional and collisionless limit, because in the collisionless limit d itself sets the Sweet–Parker layer width instead of merely determining the aspect ratio. In the initial phase, $\eta t/\delta^2\gamma_{\rm out} \ll 1$, lengthening takes the ideal form. Here simple expansion leads to $L = L_0 + v_{\rm A}t$, which is linear growth with speed $v_{\rm A}$. At each instant, stretching can be seen at the instantaneous Alfvén speed, which varies as the length changes. The ideal phases of thinning and stretching are important in a near ideal current sheet with high Lundquist number and small skin depth, which breaks up long before achieving a steady state. This is the underlying reason for Alfvén time to be critical in the analysis of plasmoid instability in forming a current sheet (Pucci & Velli 2014; Huang et al. 2017).

Numerically, we can integrate the equations to get the time evolution of the current sheet, where the initial aspect ratio is assumed to be 1.

In the ideal evolution of the current sheet, from Figure 2, stretching takes the linear form, the speed of which becomes $\frac{v_{\rm A}}{2}$. Combining $dL/dt = v_{\rm A}/2$ with the ideal evolution equation for the current sheet, we obtain for the width $\delta = \delta_0 e^{-v_{\rm A}t/(2L)}$. Compared with the situation when either length or width is fixed, the speeds of thinning and stretching both decrease, but still on the order of Alfvén time.

With the inclusion of nonideal terms, the evolution is modified; see Figures 3–5 for resistive, collisionless, and semicollisional cases, respectively.

As analyzed, nonideal effects become important as the current sheet aspect ratio increases. For nonideal plasmas, nonideal terms will play a gradually important role and eventually slow down the current sheet evolution, which reaches an asymptotic steady state. For plasmas with small nonideality, in the later stage of current sheet evolution, instability may begin to play an important role, to the extent of disrupting the current sheet before the Sweet–Parker state is reached (Pucci & Velli 2014; Comisso et al. 2016; Uzdensky & Loureiro 2016). The above picture therefore serves as a macroscopic description for current sheet evolution in the absence of instabilities and waves.

The evolution of a current sheet is presented in a pure mathematical form, which naturally raises a question about the particle density in the current sheet. At first glance, it may seem that thinning will increase the particle density of the current sheet, whereas stretching will decrease it. However, the current sheet is not a closed system. For pure stretching at the speed of Alfvén velocity, the outflow fails to carry plasmas out of the current sheet, therefore the particle is increased and the density is roughly conserved. For pure thinning, if the speed is fast, it outweighs the inflow, therefore plasma is advected out on an

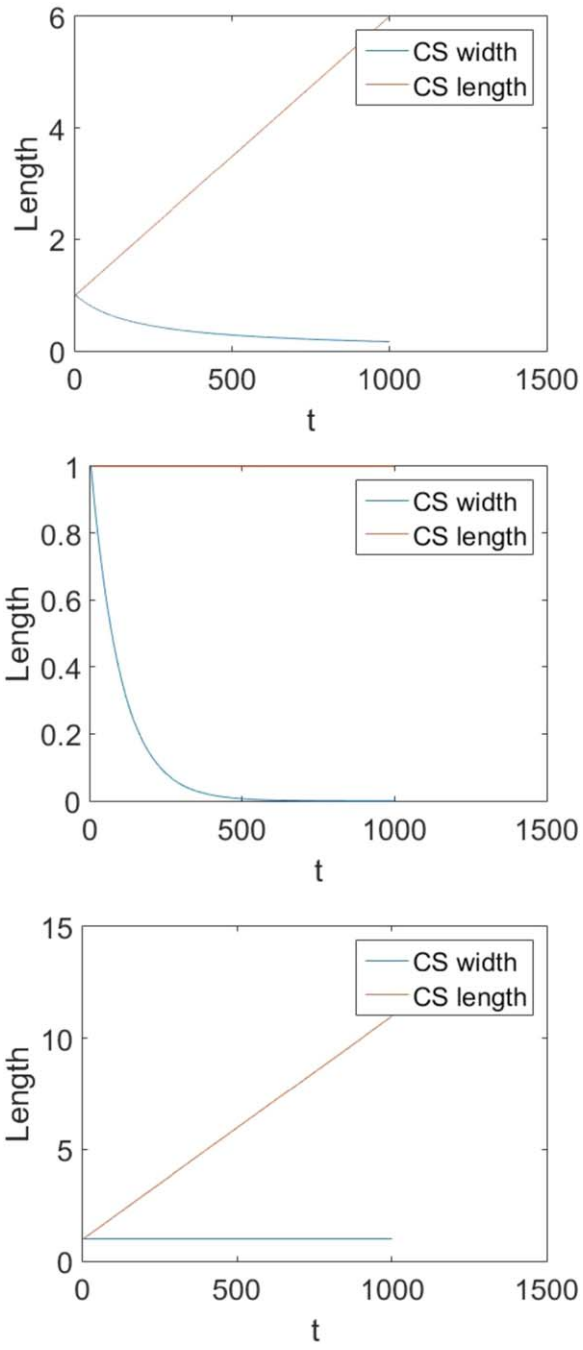

Figure 2. Evolution of an ideal current sheet (CS). From top to bottom, the images show the free-evolving, fixed length, and fixed width scenarios, respectively (the initial Alfvén time is 100).

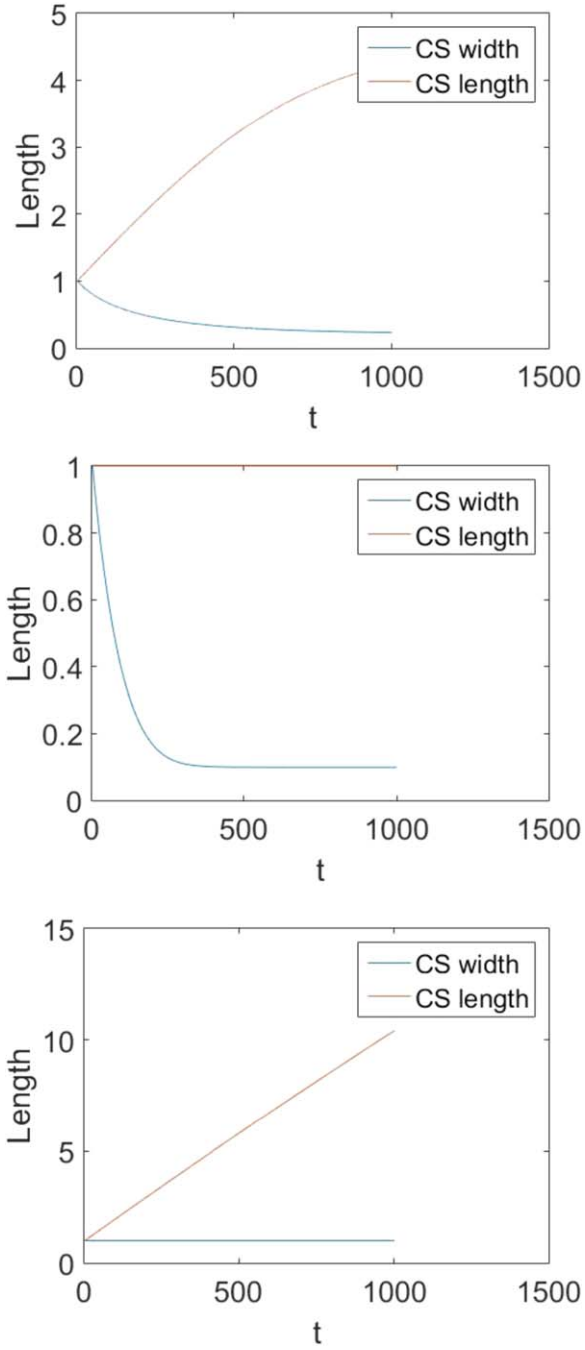

Figure 3. Evolution of a resistive current sheet. From top to bottom, the images show the free-evolving, fixed length, and fixed width scenarios, respectively (the initial Alfvén time is 100).

evolving timescale without enough of supplement. And in the free-evolving case where thinning and stretching occur simultaneously, the total area of the current sheet is roughly conserved, as is the density. Therefore, the conserved particle density is expected overall.

5. Summary

In this paper, the problem of a relativistic Sweet–Parker current sheet is investigated for pair plasmas with resistivity and thermal inertia, where the steady-state aspect ratio is found to be $\delta/L \sim (S^{-1} + d_L^2)^{1/2}$, in which the Lundquist number S is defined with respect to the four-Alfvén velocity to be able to describe the case with a highly relativistic outflow. This basic Sweet–Parker scaling is further generalized to include the influence of the ubiquitous pair processes, whose contributions can be represented by effective resistivity and the change of lepton multiplicity; the scaling relations, however, can no longer be simply represented by an effective inflow Lundquist number if there is considerable radiation energy loss.

An evolving current sheet is of more interest and is investigated in the relativistic regime. Starting from imbalanced wide current sheets, current sheet evolution is discussed in three situations, i.e., free-evolving, fixed length, or fixed width. In all cases, the initial

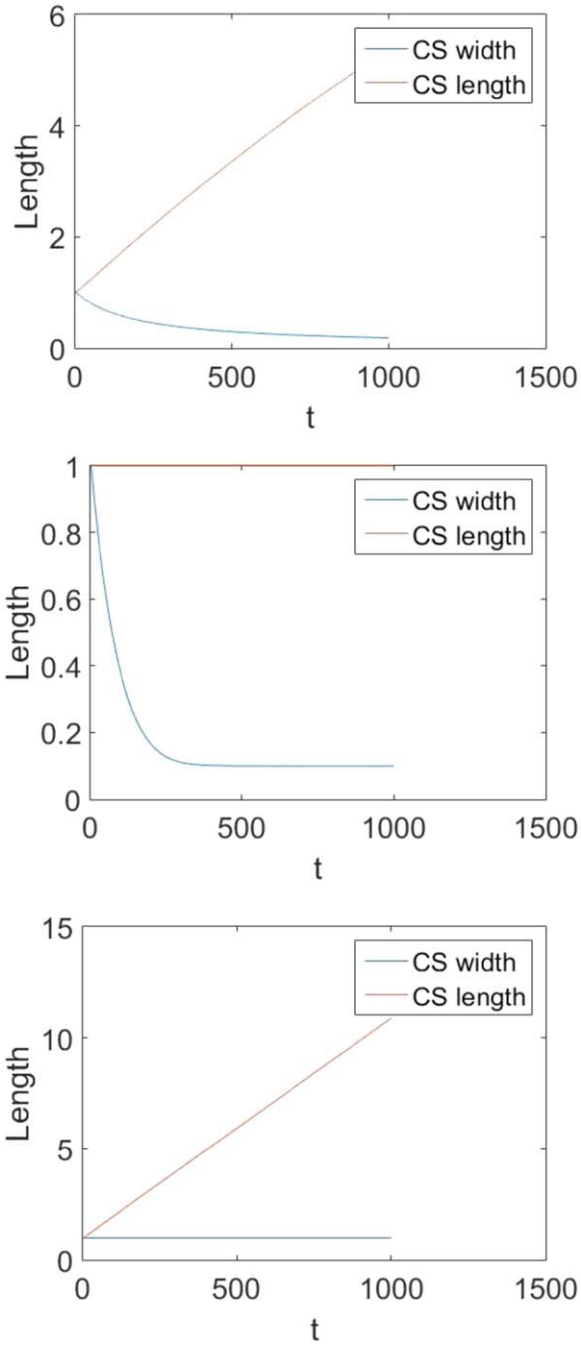

Figure 4. Evolution of a collisionless current sheet. From top to bottom, the images show the, free-evolving, fixed length, and fixed width scenarios, respectively (the initial Alfvén time is 100).

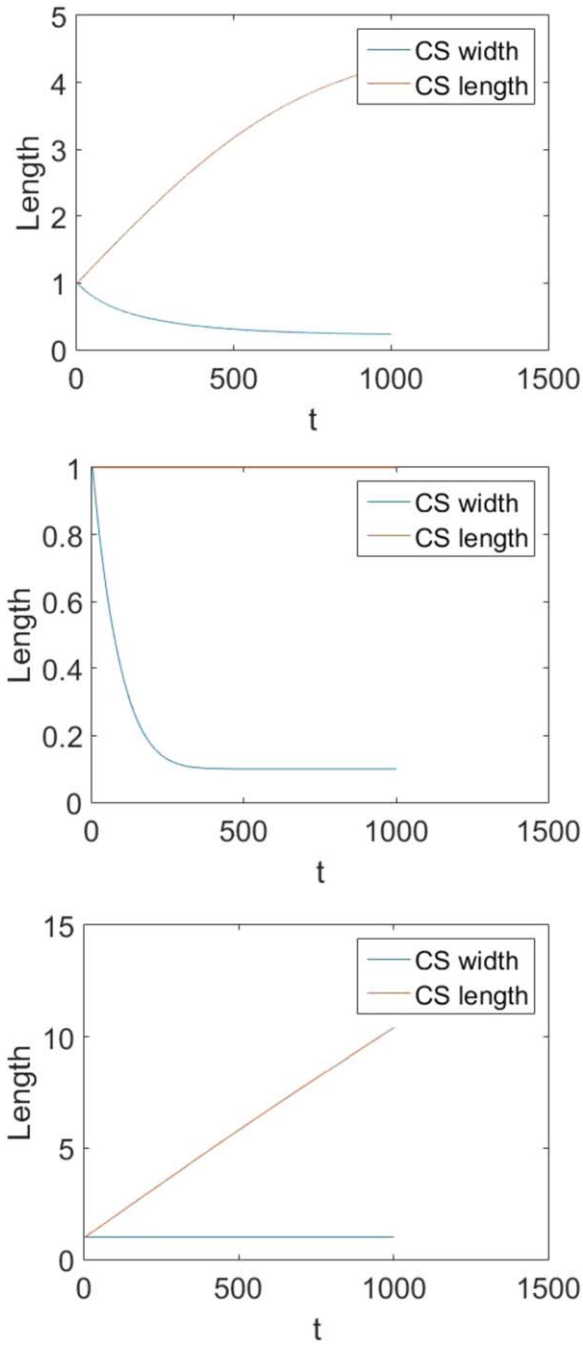

Figure 5. Evolution of a semicollisional current sheet. From top to bottom, the images show the free-evolving, fixed length, and fixed width scenarios, respectively (the initial Alfvén time is 100).

evolution takes on an ideal MHD form when the current sheet aspect ratio is much smaller than that of the Sweet–Parker steady state. Thinning is exponential at the Alfvén timescale; stretching is exponential at the instantaneous Alfvén speed, but the overall stretching is at a constant value of Alfvén velocity. Free evolution turns out to be thinning and stretching at the same time: both reduce to half the rate when the other quantity is fixed. As the aspect ratio approaches the Sweet–Parker state, both processes slow down, and reach the Sweet–Parker state asymptotically in the absence of instability and external forcing.

In real astrophysical scenarios, it remains an open question which regimes allow a Sweet–Parker current sheet to be achieved, especially when pair processes play considerable roles. Determining this requires detailed magnetic configuration and plasma dynamics. The problem of an evolving current sheet, on the other hand, is basic for a clear understanding of fast reconnection, where steady-state current sheets are always prescribed as the starting point for instabilities (Guo et al. 2014; Liu et al. 2015; Petropoulou et al. 2016), which is not true for near ideal plasma. Nonrelativistically, in the high Lundquist number regime, the onset of plasmoid instability shows up in an evolving current sheet where different forms of current sheet evolution were assumed analytically (Comisso et al. 2016; Uzdensky & Loureiro 2016) and observed numerically (Tenerani et al. 2016; Huang et al. 2017).

The investigation of current sheet evolution therefore can serve as a basis for the study of relativistic plasmoid instability and other problems situated in an evolving current sheet. Fast plasmoid instability in an evolving current sheet is a possible underlying mechanism for the impulsive reconnection and immense emission observed in astrophysics (Thompson 1994; Beckwith et al. 2008; Elenbaas et al. 2016). This will be addressed in subsequent papers.

This work is supported by the Science Challenge Project (grant No. TZ2016005), NSFC (grants No. 41674165, 11575014, and 11375053), the U.S. Department of Energy under Contract No. DE-AC02-09CH11466, and the China Scholarship Council. The author also thanks Prof. A. Bhattacharjee for helpful discussions.

ORCID iDs

S. D. Yang https://orcid.org/0000-0001-7608-8625

References

Arendt, P. N., Jr., & Eilek, J. A. 2002, ApJ, 581, 451
Arons, J. 1983, ApJ, 266, 215
Beckwith, K., Hawley, J. F., & Krolik, J. H. 2008, ApJ, 678, 1180
Beloborodov, A. M. 2017, ApJ, 850, 141
Berezhiani, V. I., Hazeltine, R. D., & Mahajan, S. M. 2004, PhRvE, 69, 056406
Bulanov, S. V. 2017, PPCF, 59, 014029
Comisso, L., & Asenjo, F. A. 2014, PhRvL, 113, 045001
Comisso, L., Lingam, M., Huang, Y.-M., & Bhattacharjee, A. 2016, PhPl, 23, 100702
Daugherty, J. K., & Harding, A. K. 1983, ApJ, 273, 761
Del Zanna, L., Papini, E., Landi, S., Bugli, M., & Bucciantini, N. 2016, MNRAS, 460, 3753
Dexter, J., McKinney, J. C., Markoff, S., & Tchekhovskoy, A. 2014, MNRAS, 440, 2185
Duncan, R. C., & Thompson, C. 1992, ApJL, 392, L9
Elenbaas, C., Watts, A. L., Turolla, R., & Heyl, J. S. 2016, MNRAS, 456, 3282
Erber, T. 1966, RvMP, 38, 626
Gedalin, M. 1996, PhRvL, 76, 3340
Giannios, D. 2010, MNRAS, 408, L46
Goodman, J., & Xu, G. 1994, ApJ, 432, 213
Guilbert, P. W., & Stepney, S. 1985, MNRAS, 212, 523
Guo, F., Li, H., Daughton, W., & Liu, Y.-H. 2014, PhRvL, 113, 155005
Harding, A. K., & Lai, D. 2006, RPPh, 69, 2631
Huang, Y.-M., Comisso, L., & Bhattacharjee, A. 2017, ApJ, 849, 75
Hurley, K., Cline, T., Mazets, E., et al. 1999, Natur, 397, 41
Joglekar, A. S., Thomas, A. G. R., Fox, W., & Bhattacharjee, A. 2014, PhRvL, 112, 105004
Kadomtsev, B. B. 1975, SvJPP, 1, 710
Kaspi, V. M., & Beloborodov, A. M. 2017, ARA&A, 55, 261
Koide, S. 2009, ApJ, 696, 2220
Koide, S., & Arai, K. 2008, ApJ, 682, 1124
Komissarov, S. S., Barkov, M., & Lyutikov, M. 2007, MNRAS, 374, 415
Kulsrud, R. M. 2005, Plasma Physics for Astrophysics (Princeton, NJ: Princeton Univ. Press)
Lazarian, A., Eyink, G. L., Vishniac, E. T., & Kowal, G. 2015, in Magnetic Fields in Diffuse Media, ed. A. Lazarian, E. M. de Gouveia Dal Pino, & C. Melioli (Berlin: Springer), 311
Lightman, A. P. 1982, ApJ, 253, 842
Liu, Y.-H., Guo, F., Daughton, W., Li, H., & Hesse, M. 2015, PhRvL, 114, 095002
Lyubarsky, Y., & Kirk, J. G. 2001, ApJ, 547, 437
Lyubarsky, Y. E. 2005, MNRAS, 358, 113
Lyutikov, M., & Uzdensky, D. 2003, ApJ, 589, 893
Manchester, R. N., & Taylor, J. H. 1977, Pulsars (San Francisco, CA: W. H. Freeman)
McKinney, J. C., & Uzdensky, D. A. 2012, MNRAS, 419, 573
Miller-Jones, J. C. A., Fender, R. P., & Nakar, E. 2006, MNRAS, 367, 1432
Parker, E. N. 1957, JGR, 62, 509
Pessah, M. E. 2010, ApJ, 716, 1012
Petropoulou, M., Giannios, D., & Sironi, L. 2016, MNRAS, 462, 3325
Priest, E., & Forbes, T. 2000, Magnetic Reconnection (New York: Cambridge Univ. Press)
Pucci, F., & Velli, M. 2014, ApJL, 780, L19
Ruffini, R., Vereshchagin, G., & Xue, S.-S. 2010, PhR, 487, 1
Sironi, L., Giannios, D., & Petropoulou, M. 2016, MNRAS, 462, 48
Sironi, L., Petropoulou, M., & Giannios, D. 2015, MNRAS, 450, 183
Sironi, L., & Spitkovsky, A. 2014, ApJ, 783, L21
Sweet, P. A. 1958, in IAU Symp. 6, Electromagnetic Phenomena in Cosmical Physics, ed. B. Lehnert (Cambridge: Cambridge Univ. Press), 123
Takahashi, H. R., Kudoh, T., Masada, Y., & Matsumoto, J. 2011, ApJL, 739, L53
Takamoto, M., Inoue, T., & Lazarian, A. 2015, ApJ, 815, 16
Tenerani, A., Velli, M., Pucci, F., Landi, S., & Rappazzo, A. F. 2016, JPlPh, 82, 535820501
Thompson, C. 1994, MNRAS, 270, 480
Thompson, C., & Duncan, R. C. 1995, MNRAS, 275, 255
Uzdensky, D. A. 2011, SSRv, 160, 45
Uzdensky, D. A., & Loureiro, N. F. 2016, PhRvL, 116, 105003
Vergani, S. D. 2007, Ap&SS, 311, 197
Werner, G. R., Philippov, A. A., & Uzdensky, D. A. 2019, MNRAS, 482, L60
Wesson, J. 1990, NucFu, 30, 2545
Yang, S.-D. 2017, PhPl, 24, 012904
Zenitani, S., & Hoshino, M. 2008, ApJ, 677, 530
Zhang, H., Li, X., Guo, F., & Giannios, D. 2018, ApJL, 862, L25
Zhong, J., Li, Y., Wang, X., et al. 2010, NatPh, 6, 984

The Astrophysical Journal, 888:128 (1pp), 2020 January 10 https://doi.org/10.3847/1538-4357/ab655e

Erratum: "Relativistic Sweet–Parker Current Sheet and Its Macroscopic Evolution" (2019, ApJ, 882, 101)

S. D. Yang[1,2]
[1] State Key Lab of Nuclear Physics and Technology and School of Physics, Peking University, Beijing 100871, People's Republic of China; sdyang@pku.edu.cn
[2] While visiting at PPPL, Princeton, NJ 08543, USA
Received 2019 December 18; revised 2019 December 20; published 2020 January 16

Figure 1 in Yang (2019) was inadvertently a duplicate of Figure 1 in Comisso & Asenjo (2014). The correct Figure 1 for Yang (2019) is provided here.

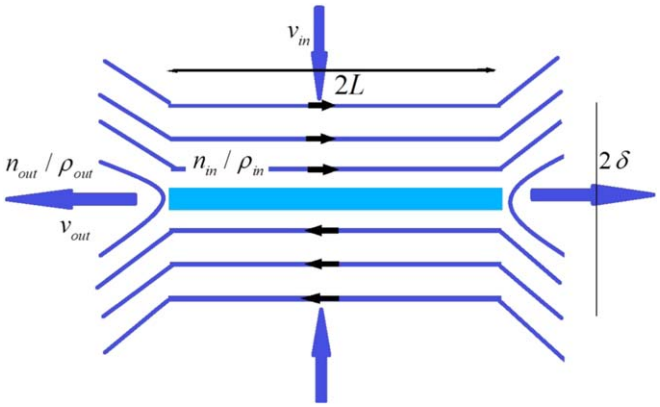

Figure 1. Sweet–Parker current sheet.

ORCID iDs

S. D. Yang https://orcid.org/0000-0001-7608-8625

References

Comisso, L., & Asenjo, F. A. 2014, PhRvL, 113, 045001
Yang, S. D. 2019, ApJ, 882, 101